




Single cell RNA-seq of human cornea organoids identifies cell fates of a developing immature cornea

George Maiti ^a, Maithê Rocha Monteiro de Barros^a, Nan Hu^a, Igor Dolgalev^b, Mona Roshan ^c, James W Foster^d, Aristotelis Tsirigos^{b,e}, Karl J Wahlin^c and Shukti Chakravarti ^{a,e,*}

^aDepartment of Ophthalmology, NYU Grossman School of Medicine, Science Building, Fifth Floor 435 E 30th, New York, NY 10016, USA

^bApplied Bioinformatics Laboratories, NYU Grossman School of Medicine, Science Building, Eighth Floor, 435 E 30th, New York, NY 10016, USA

^cUniversity of California San Diego, ACTRI Building Rm Lower level 3E419, 9452 Medical Center Drive, La Jolla, CA 92037, USA

^dWilmer Eye Institute, Johns Hopkins school of Medicine, Smith M037, 400 Broadway, Baltimore, MD 21287, USA

^eDepartment of Pathology, NYU Grossman School of Medicine, Science Building, Fifth Floor 435 E 30th, New York, NY 10016, USA

*To whom correspondence should be addressed: Email: Shukti.Chakravarti@nyulangone.org

Edited By: Bruce Levine

Classification: Major—Biological Sciences.

Minor—Medical Sciences.

Cell Biology.

Abstract

The cornea is a protective and refractive barrier in the eye crucial for vision. Understanding the human cornea in health, disease, and cell-based treatments can be greatly advanced with cornea organoids developed in culture from induced pluripotent stem cells. While a limited number of studies have investigated the single-cell transcriptomic composition of the human cornea, its organoids have not been examined similarly. Here, we elucidated the transcriptomic cell fate map of 4-month-old human cornea organoids and human donor corneas. The organoids harbor cell clusters that resemble cells of the corneal epithelium, stroma, and endothelium, with subpopulations that capture signatures of early developmental states. Unlike the adult cornea where the largest cell population is stromal, the organoids contain large proportions of epithelial and endothelial-like cells. These corneal organoids offer a 3D model to study corneal diseases and integrated responses of different cell types.

Keywords: cornea, organoid, scRNA-seq, keratoconus, FECD

Significance Statement:

There is a strong effort to develop cellular surrogates for understanding human corneal diseases. While the three major corneal cell types, epithelial, stromal keratocyte, and endothelial cells are often investigated in single monolayer cultures, their interactions in the native tissue impact their differentiation and functions. We developed 3D organoids from human-induced pluripotent stem cells to investigate the codifferentiation of corneal cells. Our single cell RNA-sequencing of human donor corneas and the organoids, shows the presence of all three cell types in the organoids and overall, their closer resemblance to developing, rather than adult corneas. These organoids, defined at the single-cell level, offer an experimental system to model human diseases in tissue culture, minimizing the need for valuable animal models.

Introduction

The cornea is the outermost transparent layer of the eye that serves as a protective barrier, and together with the lens refracts light onto the retina for visual processing (1). The third leading cause of blindness globally is due to disorders of the cornea (2), with surgical transplantation of donor cornea often the only treatment option. An estimated 12.7 million people need cornea transplantation, and only ~1 in 70 of the needs are addressed worldwide. Consequently, there is a great interest in cell-based regenerative approaches to develop treatments for blinding corneal diseases. A priori, the cornea appears to be a simple tissue of three major cell types—a stratified epithelium (3) above a basement

membrane and an acellular Bowman's layer (4), keratocytes, a specialized fibroblast-like cell type embedded in the extracellular matrix (ECM)-rich central stroma that it produces (5), and an innermost single-cell layered endothelium, which produces the Descemet's membrane, a type of basement membrane (6). It is increasingly appreciated that there is considerable heterogeneity within these three major cell types, as well as subgroups of cells with stem, progenitor, and transit amplifying qualities. Recognizing this heterogeneity, treatments for epithelial disorders, early on, have used marker-specific assessment of stemness in limbal epithelial cells (7). Comprehensive phenotyping of corneal cells by single cell RNA sequencing (scRNA-seq) can lead to better

Competing Interest: The authors declare no competing interest.

Received: January 19, 2022. **Accepted:** October 26, 2022

© The Author(s) 2022. Published by Oxford University Press on behalf of National Academy of Sciences. This is an Open Access article distributed under the terms of the Creative Commons Attribution-NonCommercial-NoDerivs licence (<https://creativecommons.org/licenses/by-nc-nd/4.0/>), which permits non-commercial reproduction and distribution of the work, in any medium, provided the original work is not altered or transformed in any way, and that the work is properly cited. For commercial re-use, please contact journals.permissions@oup.com

characterization of cell populations for such cell-based therapies. Yet, there are just a few reported examples of scRNA-seq of the cornea, with a majority of these focused on the limbal epithelial region, and very few on the central cornea (3, 8–11). Here, we performed scRNA-seq of the central human cornea to determine its epithelial, stromal, and endothelial cellular landscape. In addition, we performed scRNA-seq on human cornea organoids, and compared the organoid single cell transcriptome with that of the adult human cornea.

Organoid technology, which represents the study of 3D tissues developed from stem cells, has revolutionized the study of developmental stages and disease pathogenesis in tissue culture dishes. Many organoid studies, including our cornea organoid used induced pluripotent stem cells (iPSC). Thus, gut (12), liver (13), retina (14, 15), cornea organoids (16), and mini-cornea organoids (17) have been developed from iPSC. Another study reported development of multiple cell lineages of the eye from iPSC grown in 2D cultures (18). Multipotent somatic cells have also been used to generate corneal limbus (19) and lacrimal gland organoids (20). ScRNA-seq was used in the latter to address cellular heterogeneity of lacrimal glands (20). We performed scRNA-seq of iPSC-derived cornea organoids to elucidate their cellular complexity and relatedness to the human cornea. In our previous study of organoids, we detected major epithelial, stromal, and endothelial markers by immunohistochemistry, and the presence of collagen fibrils by transmission electron microscopy (TEM) without further characterization of the constituent cells (16, 21). Thus far, modeling of corneal diseases to investigate underlying mechanisms *in vitro* have largely relied on individual cell types, such as the epithelium and the stroma for keratoconus (22, 23), and cultured endothelial cells for Fuchs endothelial corneal dystrophy (FECD) (24). These 2D cell culture models, though invaluable, lack information about tissue development and the consequences of interactions between cell types. Clearly, there is an unmet need for 3D-corneal organoids that harbor some of the cellular complexity and functionality of the human cornea.

We compared the single cell transcriptome of the central human cornea and iPSC-derived cornea organoid keeping key features of the cornea in mind. The cornea develops from surface ectodermal cells that express the paired box transcription factor PAX6, and receives inductive signals from the lens vesicle. The epithelium becomes stratified into 6 to 8 layers postnatally (mouse) or by birth (human) with the most proliferative capacity residing in the basal layer and these proliferative basal cells are replenished from pools of limbal epithelial stem cells (3), a realization that has had vast clinical impact. Multipotent neural crest cells migrate into the space between the epithelium and the lens vesicle to produce the stromal keratocytes and the single-cell-layered endothelium (25–27). The stroma produced by the keratocytes, is composed of glycoproteins, proteoglycans, and collagen types I and V primarily that form uniformly thin collagen fibrils organized into orthogonally stacked lamellae to make up a unique ECM that is both transparent and refractive (28, 29). In a healthy adult cornea, the stromal keratocytes are quiescent and there is very little turnover of collagens and, therefore, collagen transcripts are barely detectable, although these are some of the most abundant proteins in the cornea. Perturbed by infection or injury, the keratocytes acquire gene expression programs consistent with apoptosis, cell migration and activation and ECM synthesis (30, 31). Thus, transcripts for fibrillar collagens are elevated in injured or developing corneas as shown in our earlier bulk RNA-seq of the developing and adult mouse cornea (32). The

adult corneal endothelium expresses tight junction marker ZO-1 and the Na⁺/K⁺-ATPase pump, which maintains corneal hydration for optimal vision (33). The corneal endothelium produces an acellular, collagen type VIII-rich basement membrane called the Descemet's membrane that helps to anchor the endothelium to the cornea (34). Interactions between all the three major layers are imperative for proper functioning of the cornea, underscoring the need for a 3D organoid model system. Overall, the scRNA-seq data shows strong representation of all major corneal cell types in the human iPSC-derived organoids.

Results

Major cell types in the human cornea and iPSC-derived cornea organoids

Central corneas from three human donors (Table S1), and three organoids cultured for 4 months (Figure S1), were digested separately with collagenase type 1 to prepare single cell suspension for scRNA-seq using the 10X Genomics platform. The organoids and the human corneas, six samples in all, were each sequenced individually and processed using Cell Ranger Single-Cell version 7.0.0. All subsequent analysis and integration were performed with Seurat version 4.0.4. The three organoid samples were integrated and referred to as the organoid and the three corneas as the cornea group. After extraction, the viability of cells ranged between 83% and 89% and after doublet cell exclusion, quality control filtering, a total of 25,813 from the organoids and 27,625 cells from the corneas were analyzed further (Table S2). On average we detected 3,591 and 4,885 genes per cell (Table S2), and analyzed 12 and 16 cell clusters (CL) in the cornea and the organoid, respectively (Fig. 1; Tables S3 and S4). These CL were annotated as epithelium, peripheral-limbal epithelium, stroma, corneal endothelium, immune cells, lymphatic vessel, and myofibroblasts, based on the expression of markers broadly validated for each major cell type of the ocular surface. These CL-annotation markers are summarized as expression of a gene in a CL compared to its expression in all other CL (Figure S2) and their corresponding violin plots in Figure S3. The cornea group showed a major epithelial population, a large group of stromal cells, and smaller clusters identifiable as limbal epithelial, corneal endothelium, immune cells, and myofibroblasts (Fig. 1A and C). One cornea contributed to a sizable (1,659 cells) limbal/peripheral epithelial cluster (Table S3). This is likely due to the fact that the limbal and peripheral corneal tissue is quite cell-dense, and inclusion of even a small amount of this region can yield a large number of cells. The organoid group showed a large population of epithelial-like cells, a second epithelial-endothelial like cells with a proliferating cell phenotype, and a large population of stromal-keratocyte-like cells. We detected a minor population of immune cells in both the organoid and cornea, whereas a small neural cell-like and a myofibroblast-like cluster were only found in the organoid (Fig. 1B and D; Figure S3).

The expression of the following genes supported the developmental progression of iPSC-aggregates into corneal organoids. First, the paired box 6 transcription factor (PAX6), a master regulator of epidermal cell fate in various organs, including the ocular surface ectoderm, lens vesicle, inner and outer optic cup, optic stalk, the developing and adult corneal epithelia and conjunctiva (35), was highly expressed in organoid samples, and expectedly in the epithelial/endothelial clusters of the cornea (Figure S4A). SIX3, a homeobox transcription factor that controls early eye development and is itself regulated by PAX6, was also expressed

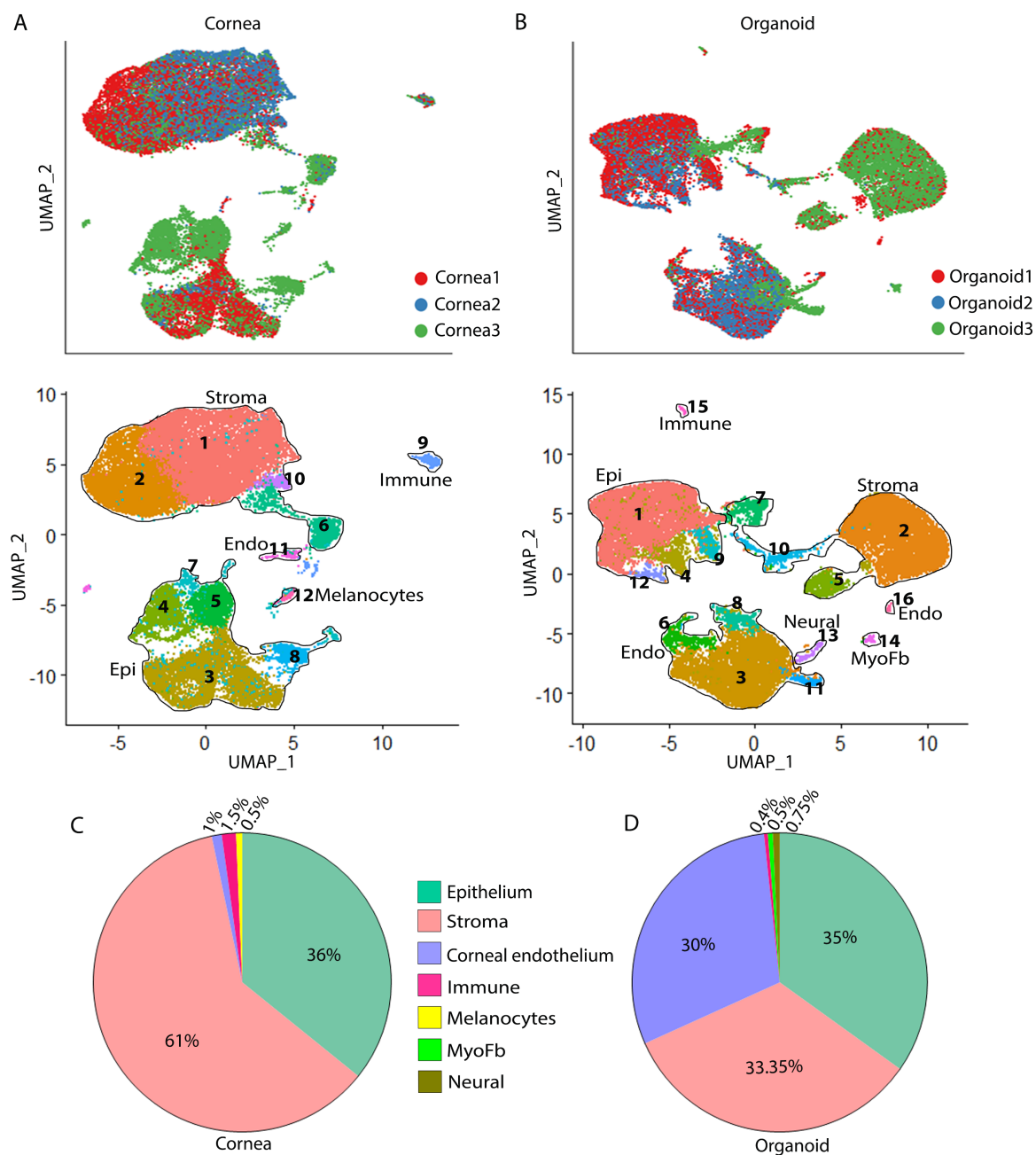


Fig. 1. Major cell-type clusters in the cornea and the organoid samples. (A) and (B) Data integration and unbiased clustering of cells from three human donor cornea and three organoid using Seurat, identified 12 clusters (CL) in the human cornea (A) and 16 CL in organoid (B). UMAP shows seven major cell types: epithelium (Epi); stroma, corneal endothelium (Endo), immune cells (immune), melanocytes, myofibroblast (MyoFb), and neural cells in the human cornea (A) and organoid (B). Relative proportions of major cell types in the human cornea (C) and organoid (D). See also Figures S2 and S3.

in the organoid epithelial CL, but its expression in the adult human cornea was limited (Figure S4B). Similarly, the *SIX3* protein, present widely in the organoid, was limited to a few epithelial cells in our adult cornea (Figure S4C). Second, as organoids differentiate, they are expected to lose the expression of undifferentiated stem cell markers like *NANOG*; indeed, *NANOG* expression was very low in the organoid (Figure S4D). Furthermore, near-absence of the retinal cone photoreceptor marker, G protein subunit alpha transducing 2 (*GNAT2*) and very low *VSX2* expression in the organoid indicated that these organoids were not retinal organoid-like (Figure S4E and S4F).

We sought experimental validation for some cornea layer-like cellular organization in the organoid. We immunostained organoid sections for the corneal epithelial cytokeratin, *KRT3* and ATP binding cassette subfamily G member 2 (*ABCG2*), and stromal markers *KERA* and collagen type V (*COL5A1*; Fig. 2A and B). The organoid showed *KRT3* and *ABCG2* immunostaining of an outer epithelial-like cell layer at the edges, and *KERA* was located in a thick stroma-like inner layer, crudely resembling the topology of the cornea. Taken together, our data indicate that organoids harbor spatially organized cellular states that represent rudimentary corneal tissue layers.

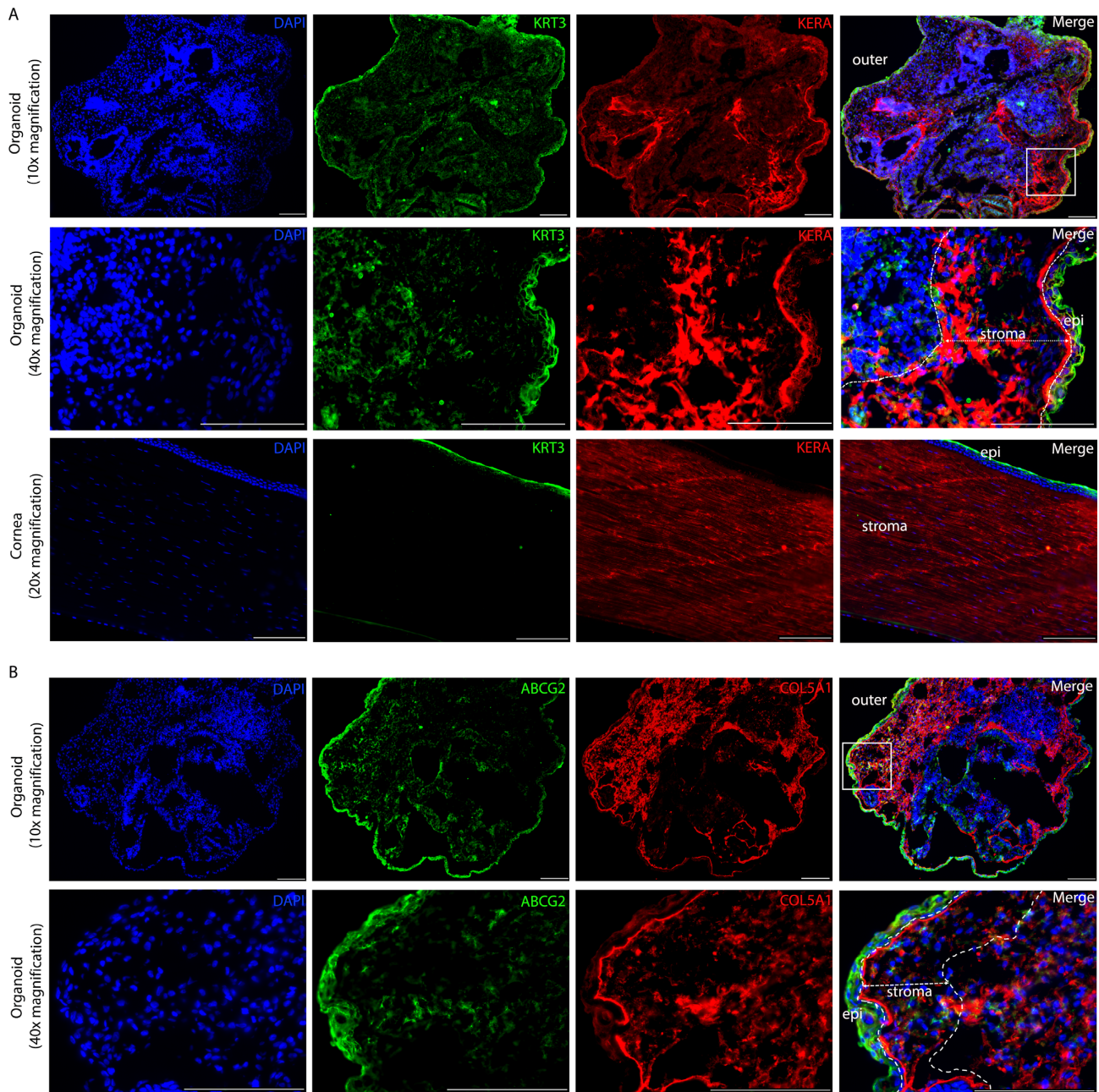


Fig. 2. Organoids display epithelial and stroma-like layers mimicking the human cornea. Immunostaining (A) of corneal epithelial marker, KRT3, co-stained with stromal marker, KERA, in the organoid and human cornea sections (bottom panels), and (B) the corneal epithelial marker, ABCG2 co-stained with stromal marker, COL5A1 in the organoid. In (A) and (B) the inset in the 10x micrograph (upper panel) is imaged at 40x in the lower. Scale bars = 133 μm .

Epithelial cell populations in the cornea and organoid

The epithelial population in the cornea showed four clusters with different expression patterns of cytokeratins (Fig. 3A–D; Figure S3C). Epithelial layers have several types of cytokeratin intermediate filaments (IF) that span through epithelial desmosomes to support cell–cell junctions, and connect to hemidesmosomes to help epithelial–basement membrane adhesion in the native cornea (36). These IFs are heterodimers of basic and acidic cytokeratin polypeptides (37, 38). KRT5/KRT14 are present in IFs of stratified squamous epithelia of the cornea and skin. We detected KRT5 expression in all corneal epithelial clusters (CL 3, 4, 5, 7, and 8), with some overlapping expression of KRT14 (Fig. 3B; Figure

S5A). A marker for undifferentiated epithelia and limbal epithelia, KRT15 (39), was expressed in the corneal CL4 (Figure S3D). In the organoid group, the large epithelial CL1, and smaller CL4, CL9, and CL12 expressed KRT5 and some KRT14, while CL1 also expressed KRT15 (Fig. 3B; Figures S3D and S5B). The KRT3 and KRT12 pair is typically expressed by differentiated corneal epithelial cells; KRT12 was expressed in corneal CL3, and KRT3 in a smaller subset, indicating the presence of basal/suprabasal differentiated epithelial cells in this cluster. Expression of KRT3 and KRT12 was very low in the organoid epithelial clusters (Fig. 3C; Tables S5 and S6). The small corneal CL7 expressed epithelial-typical genes KRT3, KRT12, KRT14, and KRT19 at low levels, as well as matrix proteoglycans DCN, KERA, and LUM, which are expressed by fibroblastic

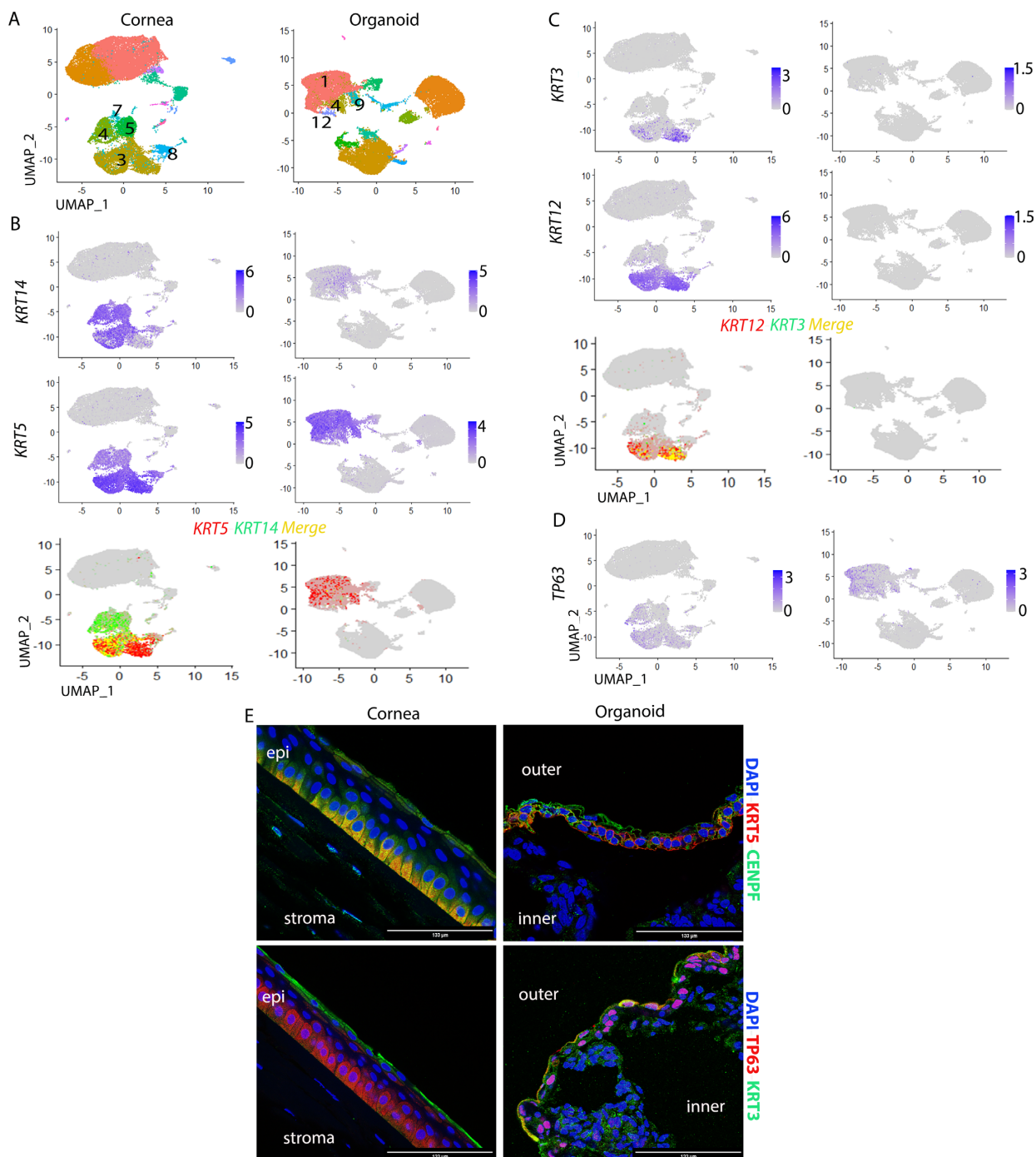


Fig. 3. Corneal epithelial-like clusters in organoids. (A) UMAP showing five epithelial CL 3, 4, 5, 7, and 8 in the cornea and four CL 1, 4, 9, and 12 in the organoid. (B) UMAP of KRT14, KRT5 and (C) KRT3 and KRT12 expressing and coexpressing cells. (D) UMAP of TP63 expressing cells. (E) Immunostaining of corneal epithelial proteins TP63, KRT3, KRT5, and CENPF in sections of the cornea and organoid. Scale bars = 133 μm. Full images and individual channels in Figure S7. See also Figures S5–S8.

cells, suggesting an epithelial–mesenchymal identity for this cluster (Figure S3C and S3E). *GPHA2*, a marker for limbal progenitor cells (8, 40) was expressed in corneal CL 4 and 5, but undetectable in the organoid (Figure S5B). The organoid epithelial CL1, and to a lesser extent CL4 and CL9 expressed TP63, a transcription factor that regulates epithelial proliferation and stratification, and considered an epithelial stem cell marker. TP63 was also expressed by the corneal epithelial CL3, CL4, and by a few cells in CL7 and CL8 (Fig. 3D). Amphiregulin (AREG), a growth factor-related marker of fully differentiated superficial corneal epithelia (8) expressed at

high levels in our corneal epithelial clusters (CL3, 4, 5, 7, and 8), was low in the organoid epithelial CL1, 4, 9, and 12 (Figure S6A).

Several mucins, *MUC1*, *MUC4*, *MUC16*, and *MUC20* (41), known to be expressed by corneal and conjunctival epithelial cells were expressed at low levels in corneal (CL8) and organoid (CL12) epithelial cells (Figure S6B). *MUC15*, encoding a membrane-associated mucin implicated in cell–matrix adhesion, and present in many epithelial tissues, was detectable in the corneal and organoid epithelial clusters. A total of two other membrane-associated mucin genes, *MUC21* and *MUC22* were expressed in the

corneal CL3 and CL8 (42) (Figure S6C). Of note, the COVID-relevant SARS-CoV-2 receptor ACE2 and the plasma membrane bound protease TMPRSS2, were expressed in the epithelial clusters in both the organoid and human cornea (Figure S6D). Previously, ACE2 and TMPRSS2 were detected in the human corneal epithelial cells (43, 44).

We validated the presence of KRT3 and KRT5 proteins in the organoid as well as sections of the human cornea by immunohistology. Anti-KRT5 stained the basal epithelial layer, while anti-KRT3 showed low punctate staining of the superficial epithelial layer in the cornea (Fig. 3E). In the organoid anti-KRT5 stained a single cell layer at the outer edge of the tissue for the most part (Fig. 3E; Figure S7A). KRT14 and KRT19 by immunostaining, colocalized in the epithelial layer of the organoid (Figure S5A). We also detected CENPF, a primary cilia protein located in the epithelial and stromal cells of the cornea, and in patches of cells in the edges of organoid (Figure S7A and S7B). CENPF mutations are associated with developmental ciliopathies, and recently, we identified CENPF variants in patients with keratoconus, a degenerative thinning disease of the cornea (45). Tp63 is known to have a cytoplasmic location in basal epithelial cells, while a more nuclear location in the few epithelial stem cells of the cornea (7). We detected cytoplasmic immunostaining of Tp63 in the basal epithelial layer of the cornea. In the organoid, Tp63 staining was detected in a layer at the edges of the organoid, with several cells showing stem cell-like nuclear staining (Fig. 3E; Figure S7C).

Epithelial cell populations compared across organoid, cornea, and skin tissues by MetaNeighbor analysis

We used MetaNeighbor analysis (46) to compare the overall likeness of the organoid with the cornea in an unbiased manner. As a noncornea tissue, we included previously published RNA-seq of three trunk skin samples of healthy subjects (47). Our combined analysis included all cell types from all three tissue types: CL with high AUROC scores were more frequent in the organoid–cornea than the organoid–skin comparison. The organoid–cornea and the organoid–organoid AUROC distribution frequencies each showed one peak with high AUROC scores indicating a large group with similar clusters (Figure S8A). AUROC scores of all comparisons are shown in Table S7. The organoid epithelial CL 4, 9, and 12 shared high AUROC scores (> 0.8) with the corneal epithelial CL4, CL5, and CL7 that generally had lower expression of the differentiated cell markers KRT3/KRT12. The organoid epithelial CL1, expressing a broad range of cytokeratins, shared similarities with the melanocyte-like corneal CL12 (AUROC score 0.74 to 0.82), the corneal stromal CL6 and two skin clusters (AUROC score 0.7 to 0.75; Table S7; Figure S8B and S8C). The organoid epithelial CL9 was similar to the corneal epithelial CL4 (AUROC score 0.77 to 0.88), CL5 (AUROC score 0.76 to 0.77), and CL7 (AUROC score 0.68 to 0.83; Table S7).

Remodeling and developing stromal ECM gene expression in the organoid compared to the corneal stromal population

The major cell type in the corneal stroma is the mesenchymal keratocyte that produces a collagen-rich ECM. The predominant collagen types in the adult healthy corneal stroma are fibrillar collagen type I (encoded by COL1A1 and COL1A2), type V (COL5A1 and COL5A2), and lesser amounts of other collagen types VI, XII, XIII, XIV, and XXIV (48). To characterize the stromal cell

population, we looked for expression of these collagens and other known stromal cell markers (Figures S3E and S9A). We detected a large (CL1 and CL2) and two other smaller stromal cell populations (CL6 and 10) in the cornea, which expressed COL1A1, COL1A2, COL5A2, and lower levels of COL5A1 (Fig. 4A and B). Matrix-degrading MMP3 was expressed by CL2, and not CL1 (Figure S3E). The small stromal cluster (CL6) was metabolically more active, expressing higher levels of type I collagen genes (COL1A1 and COL1A2) than CL1 and CL2. The organoid group displayed one large (CL2) and three other smaller (CL5, CL7, and CL10) stromal clusters. All three organoid stromal clusters showed high expression of COL1A1, COL1A2, and COL5A2 and COL5A1, with transcript levels more than 20-fold higher than the cornea. This was expected, as in the resting cornea there is very little turnover of fibrillar collagens, whereas the organoid, akin to a developing cornea, is in a stage of growth and matrix production, and thus displayed high transcriptional activities for these collagens. The presence of collagen type III in the adult healthy cornea is debatable, but it is a component of the developing and post-injury remodeling cornea (49, 50). In agreement, COL3A1 expression, minimally detectable in the corneal stromal CL6, was very high in the organoid stromal CL2, CL5, and CL10 (Fig. 4B). Immunohistology also showed extensive colocalization of collagen types III and V in stroma-like regions of the organoid (Fig. 4C; Figure S9B).

Collagen fibril-associated proteoglycans are functionally significant components of the cornea that regulate collagen fibril architecture to maintain a transparent and refractive tissue (51). These ECM proteoglycans include decorin (DCN), biglycan (BGN), lumican (LUM), and keratocan (KERA). We detected high expression of LUM and DCN in all of the corneal stromal clusters, BGN at very low levels in CL1, CL2, and CL6, and KERA expression was prominent in the larger CL1 and CL2 (Fig. 4D). To our surprise, expression of DCN was more widespread, and 10-fold higher than that of either LUM or KERA. The organoid stromal CL 2, CL5, CL7, and CL10 expressed LUM and DCN at high levels, CL2 and CL5 expressed BGN, while KERA was barely detectable (Fig. 4D; Figure S9C). However, by immunostaining the KERA protein was detectable in a stroma-like layer of the organoid (Fig. 2A). DCN immunostaining was detected in intercellular spaces in the organoid, and as known from many prior studies, along collagen fibrils in the corneal stroma (Fig. 4E; Figure S9D).

The following additional features in the organoid resonated with a developing rather than a fully mature adult cornea. First, certain ECM genes were upregulated in the organoid compared to the corneal clusters (Fig. 4F). For example, periostin (POSTN) regulates collagen fibrillogenesis and is expressed during corneal development and remodeling (32, 52). POSTN expression was elevated in the organoid stromal CL2, 5, CL7, and CL10, and not in the corneal clusters (Figure S9E). Assembly of a fibronectin (FN1) matrix precedes fibrillar collagen matrix during development (53), and Fn1 is upregulated in the developing mouse cornea compared to the adult (32). Substantial FN1 expressing cells were detected in the organoid stromal clusters (Figure S9F). SPARC, a secreted matricellular protein that regulates cell–matrix adhesion and matrix remodeling (54), was also detected at high levels in the organoid compared to the corneal stromal clusters (Figure S9G). Second, ALDH3A1, often described as corneal crystallin (55), known to increase with eyelid opening, acquisition of corneal maturity and transparency (56), was detected in the corneal epithelial and stromal clusters, and not in the organoid (Figure S9H).

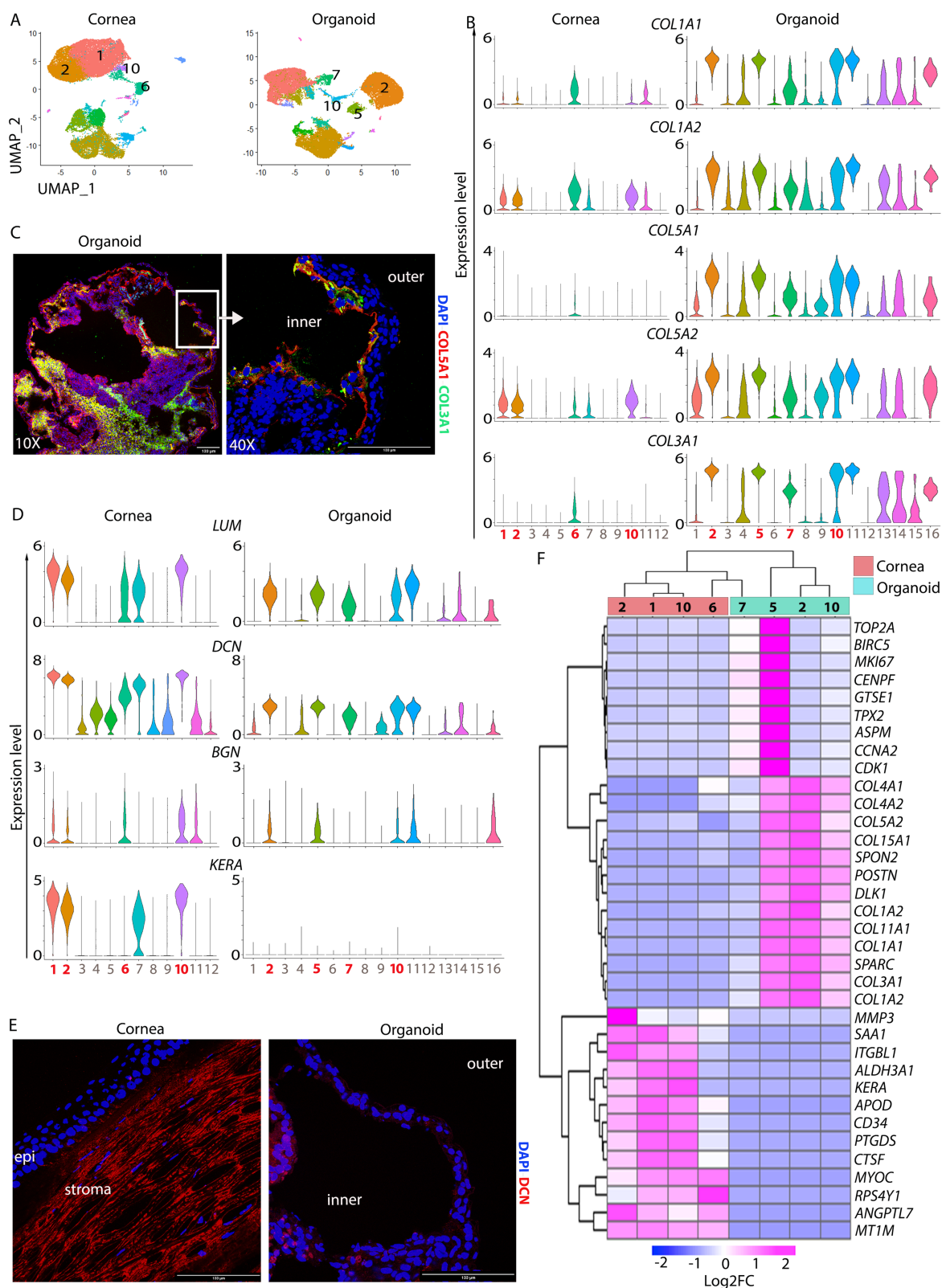


Fig. 4. Stromal cell-like clusters in organoids. (A) UMAP showing stromal CL 1, 2, 6, and 10 in the cornea, and CL 2, 5, 7, and 10 in the organoid. (B) Violin plots of Log₂ expression of COL1A1, COL1A2, COL5A1, COL5A2, and COL3A1 in the corneal and the organoid stromal CL. (C) Immunostaining of collagen types III and V in organoid sections. Scale bars = 133 μ m. (D) Log₂ expression level of stromal proteoglycans LUM, DCN, BGN, and KERA in the cornea and organoid. (E) Immunolocalization of decorin (DCN) in the corneal stroma and organoid. The organoid shows some diffused staining of DCN around cells. Scale bar = 133 μ m. Full images and individual channels in Figure S9D. (F) Expression of top 35 DEGs in all stromal CL of the cornea and organoid. Fibrillar collagen COL1A1, COL3A1, and COL5A1, basement membrane and hemidesmosomal collagen (COL15A1, COL4A1, and COL4A2) genes were upregulated in the organoid CLs. See also Figure S9.

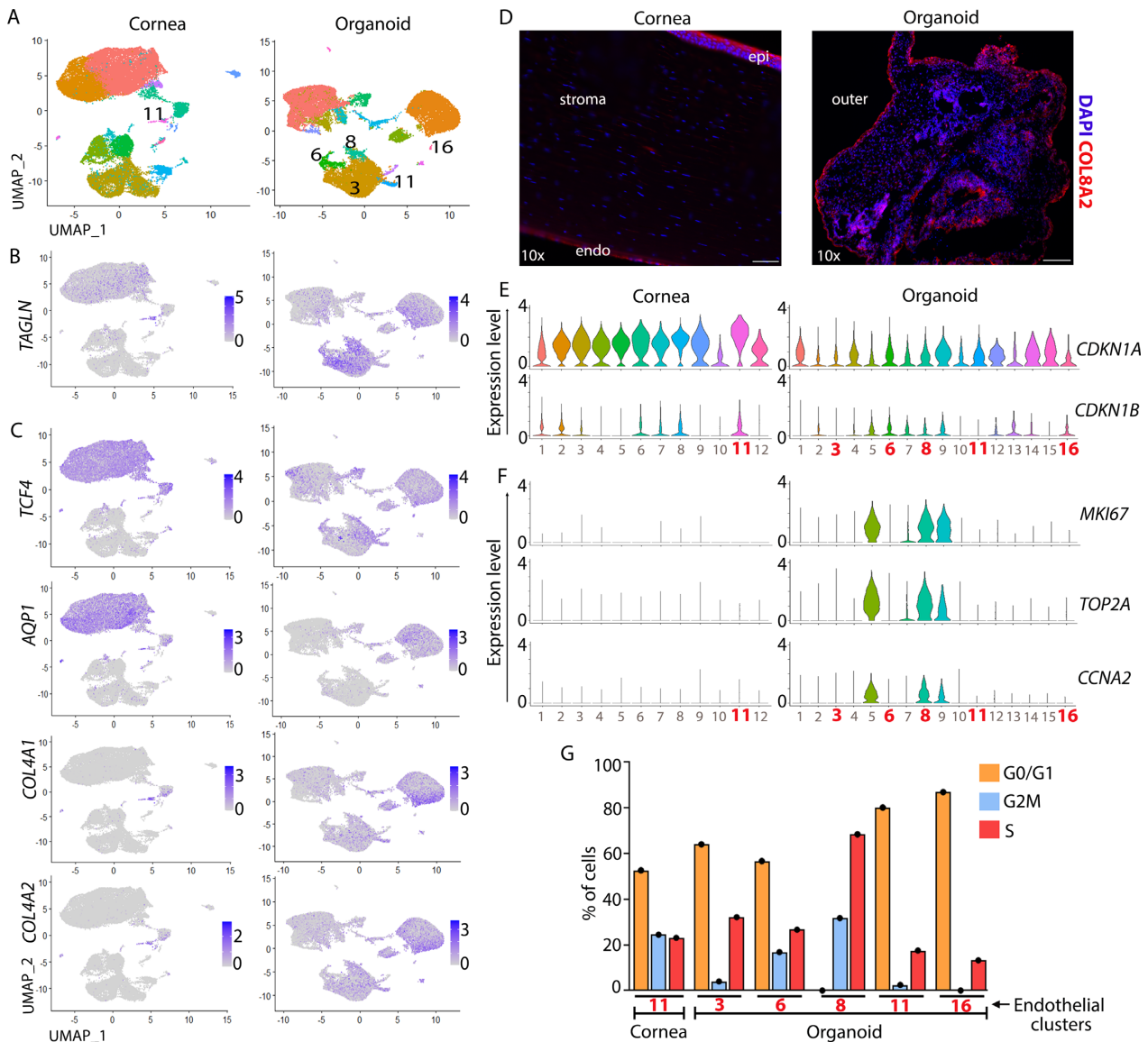


Fig. 5. Corneal endothelial-like cells in the organoid. (A) UMAP of endothelial CL11 in the human cornea and CL3, 6, 8, 11, and 16 in the organoid. (B) and (C) UMAP of corneal endothelial marker-expressing cells TAGLN (B), TCF4, AQP1, COL4A1, and COL4A2 (C). (D) Immunostaining of collagen type VIII (anti-COL8A2) in the organoid and human cornea sections. Scale bars = 133 μ m. (E) and (F) Violin plots of Log_2 expression of cell cycle regulators CDKN1A and CDKN1B, and proliferation markers MKI67, TOP2A, and CCNA2. (G) Seurat analysis of cell cycle states in the endothelial clusters indicates higher percentage of dividing cell-states (G2M and S) in the organoid CL8. See also Figure S10.

Endothelial cell types in the cornea and the organoid

The endothelium is the innermost barrier of the cornea that maintains its hydration and nutrient supply. The endothelial layer allows fluids and nutrients to leak into the cornea and actively pumps ions out to maintain an osmotic gradient for movements of fluid out of the cornea (57). It produces a combination of cell adhesion and cytoskeletal proteins, ion transporters, collagens, and basement membrane proteins that make up the Descemet's membrane. Therefore, at the transcript level there are few, if any, entirely specific markers for the corneal endothelium. We included transgelin (TAGLN) as a corneal endothelial marker. It is a cytoskeletal actin binding protein, present in the corneal endothelium and reportedly elevated in a mouse model of FECD (58) (Fig. 5A and B). Collagen type VIII is normally enriched in the endothelial cell-derived Descemet's membrane, where it creates a porous structure for nutrients to pass into the stroma,

and anchors the endothelium to the stroma (59, 60). Although collagen type VIII is also produced by the corneal epithelium and the stroma, we included it as an endothelial marker because of its functional significance in this layer. Corneal CL1, CL2, CL10, and CL11 expressed COL8A1 and COL8A2; only the CL11 transcriptome was consistent with that of a mature corneal endothelium. CL11 expressed *TJP1* (basolateral tight junction gene), TAGLN, AQP1, TCF4, ATP1A1, ATP1B1, and ATP1B3; basement membrane proteins such as NID1, NID2, LAMA5, COL4A1, and COL4A2. CL11 also expressed DCN, but not the other major stromal proteoglycans, LUM and KERA (Fig. 5C; Figure S3E and S3F). In the organoid group, several clusters (CL3, CL6, CL8, CL11, and CL16) showed a combination of endothelial, endothelial-epithelial and endothelial-stromal expression patterns. These organoid clusters expressed *TJP1*, TAGLN, TCF4, AQP1, ATP1B1, and ATP1B3, and the basement membrane COL4A1 and COL4A2 and LAMA5. Low levels of COL8A1 and COL8A2 transcripts were

detected in the organoid CL8, which we considered to be an atypical proliferating epithelial–endothelial cluster. However, anti-COL8A2 immunohistology detected the collagen type VIII protein in the outer and inner edge of organoid sections (Fig. 5D; Figure S10A).

In humans, the corneal endothelium has a finite number of mitotically quiescent, G1-arrested cells (61, 62). Quiescence is maintained by cyclin-dependent kinase inhibitors of the Cip/Kip family, p27kip1 (CDKN1B) and p21 (CDKN1A), and INK family p16INK4a (CDKN2A), which bind cyclin-CDK complexes to prevent their kinase activity in the mature endothelium (63). Consistently, CDKN1A and CDKN1B were expressed at higher levels in the corneal CL11 than the organoid endothelial-like clusters (Fig. 5E). On the other hand, cell proliferation-supportive genes *MKI67* (Ki67), *TOP2A*, and *CCNA2*, barely expressed in the corneal endothelial cells, were expressed well in the organoid epithelial–endothelial CL8 (Fig. 5F; Figure S10B). To assess cell cycle states in the endothelial population, we used the Seurat Cell cycle scoring function. The small CL8 cluster in the organoid contained a higher percentage of cells in G2M (32%) and S (68%) phase, suggesting higher proliferative cell states in this cluster (Fig. 5G).

Organoids display neural, immune, and myofibroblast-like cells but not lymphatic vessel-related- and melanocyte-like cells found in the cornea

A small cluster in the cornea (CL9, 426 cells) and the organoid (CL 15, 108 cells) expressed high levels of CC-motif chemokine ligands *CCL3*, *CCL4*, *CCL20*, *CXCL* ligands *CXCL3* and *CXCL8*, and *IL1B* genes suggesting an immune cell identity for these (Fig. 6A; Figure S3G). Unlike the organoid CL15, the corneal CL9 expressed MHCII genes *HLA-DQA1*, *HLA-DRB1*, and *HLA-DRA*, consistent with an antigen presenting monocyte, macrophage, and dendritic cell identity. By contrast, the organoid in CL15 expressed high levels of *FUCA1*, encoding the lysosomal alpha-L-fucosidase 1, *PLA2G7* (phospholipase A2 group VII), and *ACSL4* (acyl-CoA synthetase long chain family member 4) typically produced by granulocytes (Fig. 6B; Figure S11A).

Myofibroblasts facilitate corneal healing after trauma, infections, and surgeries, and thus beneficial, but they can also cause vision-debilitating haze and fibrosis (64). No myofibroblast-like cells were detected in the cornea, while a small cluster (CL14) in the organoid expressed cytoskeletal genes actin (*ACTA2*), titin (*TTN*), and myosin subunit-encoding *MYH6*, *MYL3*, *MYL4*, and *MYLK*, and troponin genes *TNNT2* (65) (Fig. 6C and D; Figure S3I and S11B). The lymphatic vessel markers *CCL21*, *LYVE1*, and *CLDN5* were expressed in a small subset of CL7 in the cornea, but absent in the organoid (Fig. 6E and F). Furthermore, a small cluster (CL12) of 185 cells (Table S3) in cornea expressed pigmented cell markers *TYRP1*, *MLANA*, *DCT*, *PMEL*, *TRPM1*, and *TYR* (Figures S3J and S11C), thus defining this cluster as melanocytes. However, these pigmented cell markers were undetectable in the organoid. On the other hand, the small organoid CL13 (196 cells, Table S4) expressed neural cell markers (*DCC*, *NNAT*, *NRXN1*, and *CNTNAP2*) which were not detected in the cornea (Figure S11D).

Discussion

In this study, we performed concurrent scRNA-seq analyses of three human iPSC-derived cornea organoids and full-thickness central corneas from three different adult human donors. Our human corneal dataset corroborated recent transcriptomic

studies of the full thickness human cornea (10, 44). Human cornea organoids have not been analyzed at the single cell transcriptomic level. Here, we show the repertoire of cornea-like cells present in the organoid. As a whole, the organoid displayed features of a developing or a healing cornea. In two earlier studies of the cornea, Ligocki et al. (10), discussed 16 distinct clusters, and Collin et al. (8), discussed 21 clusters in the cornea and adjacent conjunctival tissue. We identified four distinct epithelial, one limbal, four stromal clusters, and one corneal endothelial cluster. Hallmark genes of the epithelium (*PAX6*, *KRT3*, and *KRT12*), stroma (*DCN*, *KERA*, and *LUM*) and the endothelium (*AQP1*, *TJP1*, *COL8A1*, and *COL8A2*) were detected in our adult donor human corneas. All major ECM genes in the two reported studies were represented in our data. The scRNA-seq data from the organoid indicated the presence of all major cornea-like cell types. Additionally, markers of the undifferentiating iPSC cells (*NANOG* and *OCT4*) were no longer detectable in the organoid, indicating its progression into differentiated cell fates.

A number of observations indicated a closer resemblance of the organoid to developing and immature, more so than the adult cornea. First, *PAX6*, that helps to define the eye field and early embryonic development (66), was highly expressed in the organoid. *SIX3*, a member of the homeobox transcription factor, known to suppress WNT signaling and regulate *PAX6* to promote eye development, showed high *PAX6*-overlapping expression in the organoid, and as expected, little to no expression in our adult corneal CL. The human cornea continues to grow and mature for at least 6 months after birth, at which time it is influenced by various developmental signals as well as external cues. The major events in the developing cornea include stratification of the squamous epithelial cells, increase in stromal matrix deposition and a decline in endothelial cell density (25, 26, 67, 68). The gene expression pattern of the organoid group conformed to this general developmental scheme. Expression of *KRT5* and *KRT14* in the organoid indicated the presence of less differentiated basal and suprabasal-like cells. *KRT12*, a marker for differentiating stratified corneal epithelium (69), was not detectable in the organoid. High expression of several cell growth factors (*GPC3*, *IGF2*, *FSTL1*, *EGF*, and *EID1*) and cell proliferation genes (*MKI67*, *CENPF*, and *TOP2A*) also supported the active cell growth and proliferative state of the organoid analogous to immature developing corneas. Second, many ECM genes are transcriptionally more active in the developing cornea although at a protein level they make up the bulk of the adult cornea. In this respect the organoid showed closer resemblance to a developing cornea. Type IV collagen, is an abundant basement membrane collagen in the adult cornea, but transcripts for *COL4A1* and *COL4A2* were present at very low levels in corneal epithelial CL, because its turnover in the adult healthy cornea is low. The organoid CL on the other hand showed robust expression of *COL4A1* and *COL4A2* as reported for infant human corneas (70). The ECM collagen types I and V are the most abundant proteins of the corneal stroma, yet the adult corneas showed very low levels of the respective transcripts. Again, these collagens are highly stable with little turn over in a homeostatic cornea. Corroboratively, in our earlier transcriptomic study of the postnatal day 10 and the adult mouse cornea the transcripts for collagen types I and V were markedly elevated in the postnatal cornea compared to the adult (32). In the same vein, here we noted the organoid stromal CL to have high levels of transcripts for *COL1A1*/*COL1A2* and *COL5A1*/*COL5A2*, as well as *COL3A1* that encodes for type III collagen, which is typical of the immature and injured cornea. Elevated *POSTN* in the organoid was also consistent with its role in collagen fibrillogenesis and stromal maturation (71).

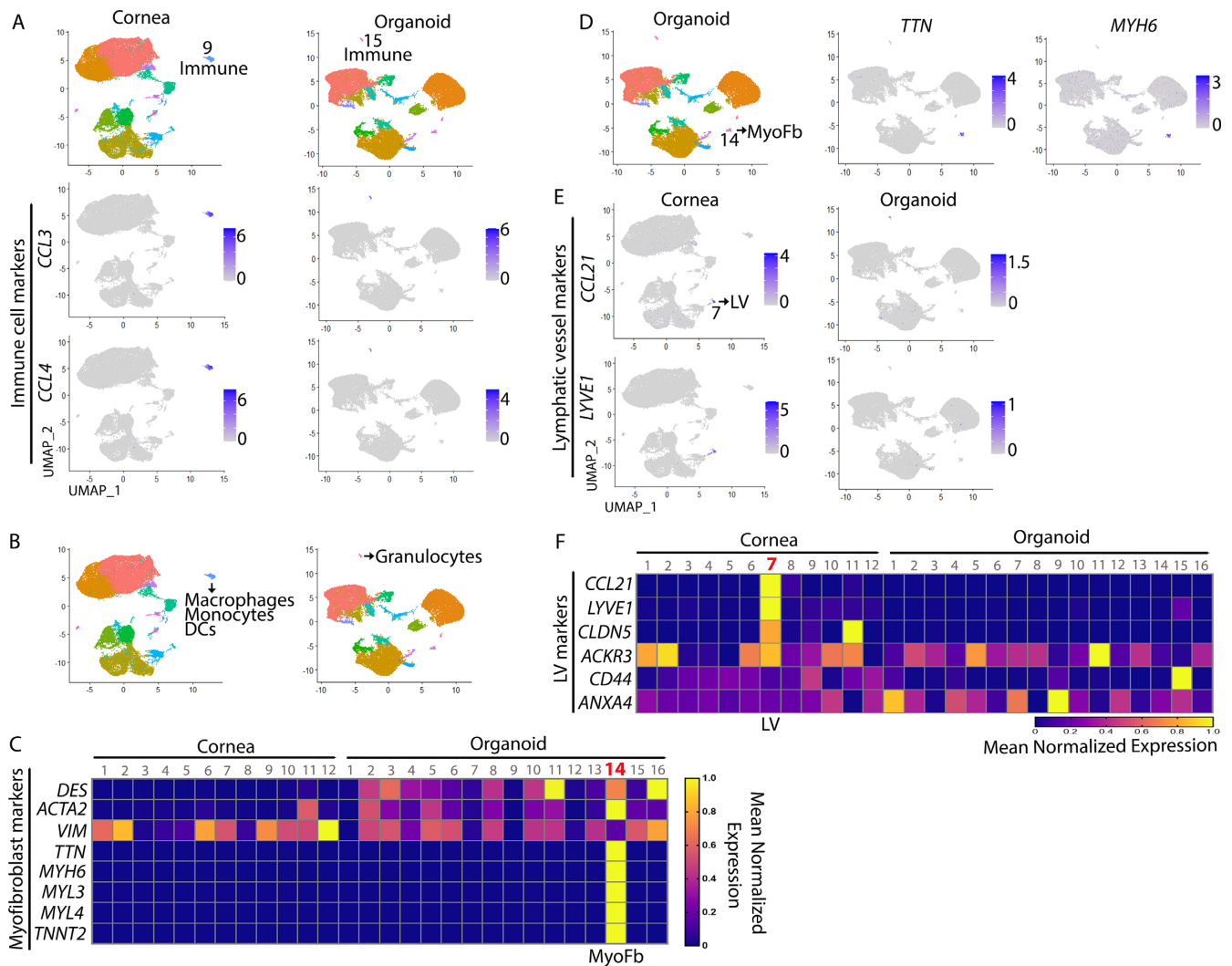


Fig. 6. Immune and myofibroblast-like CLs in the organoid. (A) UMAP of immune cell markers *CCL3* and *CCL4* in corneal CL9 and organoid CL15. (B) Cells originating from the cornea in CL9 fit the expression profile (Figure S11A) of macrophages, monocytes, and DCs, and those originating from the organoid CL15 are similar to granulocytes. (C) Heatmap of myofibroblast gene expression. (D) UMAP of myofibroblastic CL14 in the organoid. (E) UMAP of lymphatic vessel marker *CCL21* and *LYVE1* expressing cells in the subset of CL7 in cornea. (F) Heatmap showing high expression of lymphatic vessel markers in corneal CL7. See also Figure S11.

Our findings show that overall human iPSC-derived cornea organoids harbor cell types found in the human cornea. An unbiased comparison of the organoid with our corneal data and a previously published human skin study (47) indicated greater similarities (higher AUROC scores) between epithelial clusters of the cornea and the organoid than that of the skin. However, there were small clusters in the organoid that shared similarities with a few skin-CL. Immunohistology of the organoids revealed organization of epithelial-marker and stromal-marker expressing cells in adjacent layers—a rudimentary representation of corneal layers. In our previous morphological study, we had matured the organoids for up to 7 months where we demonstrated simple lamellar organization of collagen fibrils by TEM (16), a stronger indication of their corneal nature.

In the current study, the three organoids were biological replicates, yet two had stronger representation of epithelial and endothelial cells while the third a more stroma-rich phenotype. During corneal organoid maturation in culture, we attempt to recreate conditions that resemble an eye-field development. Early cell decisions during this process can reinforce

the epithelial/endothelial fate, causing the corneal organoids to be epithelial-leaning and somewhat stromal-cell poor or vice versa. We realize the stochastic nature of these early cell-fate decisions, but our previous morphological studies of the organoids could not have provided this insight. Additional standardizations, and sequencing of larger batches are, thus required to determine whether the cornea organoids consistently bifurcate to produce epithelial/endothelial-rich or stromal-cell rich organoids. Alternatively, whether longer maturation or further adjustments of the conditions may yield strong epithelial/endothelial and stromal cell contributions in the same organoid.

Development of iPSC-derived cornea organoids is the first step toward a cell culture model, where the role of specific genes in the cornea may be studied during codifferentiation of corneal cell types. While SARS-CoV-2 was not the focus of the current study, coexpression of *ACE2* and *TMPRSS2* in the organoid supports its suitability to model SARS-CoV-2 infection and study the accompanying cellular and molecular changes as well. The cornea organoids may be used in functional studies of genes potentially

involved in cell–cell and cell–ECM adhesion and tissue-level organization during early corneal development.

Materials and Methods

iPSC maintenance

The IMR90.4 cell line was obtained from WiCell (Madison, Wisconsin) and grown at UC San Diego with IRB approval. The cells were maintained in antibiotic free media on 1% (vol/vol) Matrigel-GFR (#354230; BD Biosciences) coated dishes at 37°C under hypoxic conditions (10% CO₂/5% O₂) in mTeSR1 (StemCell Technologies). These were passaged every 4 to 6 days with Accutase (#A6964; Sigma) for 8 to 10 min, dissociated to single, quenched in mTeSR1 plus 5 μM (-) blebbistatin (B; #B0560; Sigma), pelleted at 80 *g* for 5 min, and resuspended in mTeSR1 + B and plated at 5,000 cells per 35 mm dish as described earlier (15, 16, 21).

Human corneal organoid differentiation

The iPSC-derived corneal organoids were cultured and matured as previously described (15, 16, 21). Briefly, 1,000 to 3,000 iPSCs in 50 μl of mTeSR1 + B were seeded per well in polystyrene 96-well U-bottom plates (#650180; Greiner). The aggregates were transitioned to neural induction medium (BE6.2-NIM) by adding 50 μl of BE6.2 + 2% MG on day 1 and 50 μl of BE6.2 + 2% MG each day for 4 days. Between days 4 and 8, approximately 50% of the medium exchange (100 μl) was replaced daily. Between days 1 and 6, we added 3 μM of the WNT antagonist (IWR-1-endo; #681669; EMD Millipore). Between days 10 and 12, the organoids were grown in BE6.2 + 300 nM Smoothed agonist (SAG; #566660; EMD Millipore), then LTR + SAG between days 12 and 18. Optic vesicles were excised as previously described (15, 16). Around day 31, the corneal organoids have a translucent cyst-like appearance and were allowed to mature in culture for ~ 4 months.

Single-cell isolation

Three cadaverous donor human corneas (Table S1)) were received from the Lions Eye Institute for Transplantation and Research, Tampa, Florida. The central region of the human corneas were cut into small pieces and digested in 2 ml of digestion mix: 2 mg/ml collagenase type 1 (#SCR103; EMD Millipore) in DMEM-F12 supplemented with 5% FBS (#10438026; Gibco), 1% antibiotic-antimycotic (#15240062; Gibco), 1 mM L-ascorbic acid using rotatory nutator at 37°C for 6 h at 5% CO₂. The supernatant was collected by allowing the undigested tissue to settle under gravity every 2 h and this was repeated 2 to 3 times. The collected supernatant samples were stored on ice at all stages and pooled after a final 6 h of digestion, and centrifuged at 500 *g* for 5 min. The supernatant was discarded and the pellet resuspended in 5 ml of 1x Accutase and incubated at 37°C for 20 min in a 5% CO₂ incubator. Fresh 5 ml of DMEM-F12 with 5% FBS was added and passed through a 40-μm cell strainer and centrifuged at 500 *g* for 5 min/4°C. Supernatant was discarded and the pellet resuspended in PBS with 0.04% BSA or complete DMEM-F12 to make a single cell suspension. Live cells were counted by trypan-blue exclusion in a Countess II automated cell counter.

Single-cell library preparation and sequencing

A total of six individuals (three organoids and three human corneas) cDNA libraries were prepared using the Chromium Single Cell 3' Library & Gel Bead Kit v2 (10x Genomics) and sequenced using an Illumina HiSeq 4000 as 150-bp paired-end reads.

Preprocessing of scRNA-seq data and analysis

The sequence results were demultiplexed and converted to FASTQ format using the Illumina bcl2fastq software. The 10x Genomics Cell Ranger Single-Cell Software Suite v7.0.0 was used for sample demultiplexing, barcode processing, single-cell 3' gene counting, and mapping to the Human References GRCh38-2020-A (2020 July 7). Meaningful reads were calculated using (1) valid barcodes; (2) valid unique molecular identifier (UMI); (3) associated with a cell barcode; and (4) confidently mapped to exons (72). Only confidently mapped, non-PCR duplicates with valid barcode and UMIs were used to generate gene–cell-barcode matrices for the cornea and organoid samples (Table S2). The Cell Ranger data output was analyzed using the Seurat R package v 4.0.4 (73, 74). Low-quality cells > 10,000 and < 1,000 detected genes, as well as cells showing > 10% mitochondrial gene content were removed from the analysis. The data was normalized and scaled using the “Log-Normalize” and the “ScaleData” Seurat functions. Highly variable genes were selected using the “FindVariableFeatures” function for downstream analysis. PCA was performed and dataset dimensionality was reduced by selecting the first 20 principal components. Clusters of cells were identified for the cornea and the organoid using the “FindNeighbors” and “FindClusters” functions. We chose the resolution parameter of 0.2, which identified 12 and 16 biologically meaningful clusters in the cornea and the organoid, respectively. The cells and clusters were visualized in 2D using uniform manifold approximation and projection (UMAP) plots. DEGs were found for each cluster for both the cornea and the organoid dataset individually using the “FindAllMarkers” function. Clusters were manually marked and identified based on known markers of corneal structures. The cornea and organoid datasets were integrated by selecting the top scoring features from both datasets with the “SelectIntegrationFeatures” function, followed by “FindIntegrationAnchors” to find a set of anchors between the datasets that were used to finally integrate the objects using the “IntegrateData” function (74).

We performed a MetaNeighbor analysis (46) of our cornea, organoid, and a previously published skin data as follow. Three healthy human trunk skin tissue RNA-seq data (EGAD00010001620) from Cheng et al. (47) were used to extract BAM files, which were converted to unaligned reads files (FASTQ) using the bamtofastq function at default settings in Cell Ranger v7.0.0. We then created Seurat object from the raw barcode matrix by Seurat read10x function and performed quality checks as described before. The skin data was taken through the analysis steps as outlined before for the cornea and the organoid data. We used MetaNeighbor’s mergeSE function to combine three integrated datasets into a single object. In order to obtain the best result, we selected highly variable genes across datasets by the variableGenes function. Lastly, we used MetaNeighborUS function for unsupervised testing and returned a cell-type-by-cell-type matrix containing cell type similarities as AUROC scores. We extracted all similarity scores between all clusters in the organoid except itself; all clusters in cornea and all clusters in the skin data.

Tissue preparation and immunofluorescence staining

The organoids were fixed in 4% paraformaldehyde for 4 h at 4°C, rinsed with 1x PBS, followed by overnight incubation in 10%, 20%, and 30% sucrose at 4°C with shaking. After removing the extra sucrose, the organoids were embedded into OCT-containing molds on dry ice and stored in –80°C. The unfixed human donor corneas

were directly placed into OCT-molds on liquid nitrogen and stored in -80°C . The frozen sections were air dried for 1 h and fixed in 4% PFA for 15 min. The 100- μm organoid and human cornea sections were permeabilized with 0.1% Triton X-100 in PBS for 5 min at room temperature (RT). Followed by two washes with PBS and blocked using 3% BSA, 5% normal goat serum in PBS (blocking buffer) for 1 h. Primary antibodies were diluted in 1x PBS with 0.05% Tween-20 (PBST) at appropriate concentrations and slides were incubated for overnight at 4°C in a humidified chamber. Slides were then washed 3×5 min with PBST and incubated with secondary antibodies diluted in blocking buffer for 1 h at RT. Followed by washing 3×5 min with PBST and counterstained with 1 $\mu\text{g}/\text{ml}$ DAPI (#564907; BD Biosciences) for 2 min. Slides were washed twice with ice-cold 1x PBS to remove extra DAPI and mounted in antifade mounting media (#H-1000; Vector Laboratories) with coverslips. The slides were visualized using Zeiss LSM-700 laser scanning confocal microscope and images were analyzed using Fiji. Primary and secondary antibody details can be found in Table S8.

Acknowledgments

We thank Drs. Jesse Gillis and Leon French for their insightful comments on MetaNeighbor analysis. We thank the Genome Technology Center (GTC) for library preparation and sequencing, and the Applied Bioinformatics Laboratories (ABL) for providing bioinformatics support and analysis of the data (grant P30CA016087 at the Laura and Isaac Perlmutter Cancer Center) and the computing resources at the NYU School of Medicine High Performance Computing (HPC) Facility. We also thank the following NYU laboratories: Experimental Pathology Research Laboratory for tissue sectioning and Microscopy Laboratory for confocal imaging.

Supplementary Material

Supplementary material is available at [PNAS Nexus](#) online.

Funding

This work was funded by the NIH grants R01EY030917 and R01EY026104 to S.C. and the Research to Prevent Blindness unrestricted funds to the NYU Department of Ophthalmology. The study was also supported by R01EY031318 and R21EY031122 to K.J.W.

Authors' Contributions

Conceptualization: S.C. and G.M. Investigation: G.M. and S.C. Supervision: S.C. Methodology: G.M., S.C., K.J.W., M.R.M.B., and J.W.F. Bioinformatics and computational analysis: G.M., M.R.M.B., N.H., I.D., and A.T. Writing—original draft: G.M. and S.C. Writing—review and editing: S.C., G.M., M.R.M.B., and K.J.W.

Data Availability

Single cell RNA sequencing data have been deposited in the National Center for Biotechnology Information GEO database (accession no. GSE218123).

References

- Maurice DM. 1957. The structure and transparency of the cornea. *J Physiol*. 136:263–286.
- WHO. 2019. World report on vision. Geneva: World Health Organization; 2019. Licence: CC BY-NC-SA 3.0 IGO.
- Lavker RM, Kaplan N, Wang J, Peng H. 2020. Corneal epithelial biology: lessons stemming from old to new. *Exp Eye Res*. 198:108094.
- Wilson SE. 2020. Bowman's layer in the cornea - structure and function and regeneration. *Exp Eye Res*. 195:108033.
- Etheredge L, et al. 2010. Enhanced cell accumulation and collagen processing by keratocytes cultured under agarose and in media containing IGF-I, TGF- β or PDGF. *Matrix Biol*. 29:519–524.
- de Oliveira RC, Wilson SE. 2020. Descemet's membrane development, structure, function and regeneration. *Exp Eye Res*. 197:108090.
- Pellegrini G, et al. 2001. p63 identifies keratinocyte stem cells. *Proc Natl Acad Sci USA*. 98:3156–3161.
- Collin J, et al. 2021. A single cell atlas of human cornea that defines its development, limbal progenitor cells and their interactions with the immune cells. *Ocular Surf*. 21:279–298.
- Dou S, et al. 2021. Molecular identity of human limbal heterogeneity involved in corneal homeostasis and privilege. *Ocular Surf*. 21:206–220.
- Ligocki AJ, et al. 2021. Molecular characteristics and spatial distribution of adult human corneal cell subtypes. *Sci Rep*. 11: 16323.
- Li JM, et al. 2021. Single-cell transcriptomics identifies a unique entity and signature markers of transit-amplifying cells in human corneal limbus. *Invest Ophthalmol Vis Sci*. 62:36.
- Spence JR, et al. 2011. Directed differentiation of human pluripotent stem cells into intestinal tissue in vitro. *Nature*. 470:105–109.
- Ramli MNB, et al. 2020. Human pluripotent stem cell-derived organoids as models of liver disease. *Gastroenterology*. 159:1471–1486.e1412.
- Zhong X, et al. 2014. Generation of three-dimensional retinal tissue with functional photoreceptors from human iPSCs. *Nat Commun*. 5:4047.
- Wahlin KJ, et al. 2017. Photoreceptor outer segment-like structures in long-term 3D retinas from human pluripotent stem cells. *Sci Rep*. 7:766.
- Foster JW, et al. 2017. Cornea organoids from human induced pluripotent stem cells. *Sci Rep*. 7:41286.
- Susaimanickam PJ, et al. 2017. Generating minicorneal organoids from human induced pluripotent stem cells. *Development*. 144:2338–2351.
- Hayashi R, et al. 2016. Co-ordinated ocular development from human iPS cells and recovery of corneal function. *Nature*. 531:376–380.
- Higa K, et al. 2020. Human corneal limbal organoids maintaining limbal stem cell niche function. *Stem Cell Res*. 49:102012.
- Bannier-Hélaouët M, et al. 2021. Exploring the human lacrimal gland using organoids and single-cell sequencing. *Cell Stem Cell*. 28:1221–1232.e1227.
- Foster JW, Wahlin KJ, Chakravarti S. 2020. A guide to the development of human cornea organoids from induced pluripotent stem cells in culture. *Methods Mol Biol*. 2145:51–58.
- Foster JW, et al. 2018. Integrated stress response and decreased ECM in cultured stromal cells from keratoconus corneas. *Invest Ophthalmol Vis Sci*. 59:2977–2986.
- Sharif R, Hjortdal J, Sejersen H, Frank G, Karamichos D. 2017. Human in vitro model reveals the effects of collagen cross-linking on keratoconus pathogenesis. *Sci Rep*. 7: 12517.
- Liu C, Vojnovic D, Kochevar IE, Jurkunas UV. 2016. UV-A irradiation activates Nrf2-regulated antioxidant defense and induces

- p53/caspase3-dependent apoptosis in corneal endothelial cells. *Invest Ophthalmol Vis Sci.* 57:2319–2327.
25. Hay ED. 1980. Development of the vertebrate cornea. *Int Rev Cytol.* 63:263–322.
 26. Graw J. 2010. Eye development. *Curr Top Dev Biol.* 90:343–386.
 27. Lwigale PY. 2015. Corneal development: different cells from a common progenitor. *Prog Mol Biol Transl Sci.* 134:43–59.
 28. Quantock AJ, Young RD. 2008. Development of the corneal stroma, and the collagen-proteoglycan associations that help define its structure and function. *Dev Dyn Off Publ Am Assoc Anatom.* 237:2607–2621.
 29. Chakravarti S, Zhang G, Chervoneva I, Roberts L, Birk DE. 2006. Collagen fibril assembly during postnatal development and dysfunction regulation in the lumican-deficient murine cornea. *Dev Dyn Off Publ Am Assoc Anatom.* 235:2493–2506.
 30. Mohan RR, et al. 2003. Apoptosis, necrosis, proliferation, and myofibroblast generation in the stroma following LASIK and PRK. *Exp Eye Res.* 76:71–87.
 31. Chakravarti S, Wu F, Vij N, Roberts L, Joyce S. 2004. Microarray studies reveal macrophage-like function of stromal keratocytes in the cornea. *Invest Ophthalmol Vis Sci.* 45:3475–3484.
 32. Wu F, Lee S, Schumacher M, Jun A, Chakravarti S. 2008. Differential gene expression patterns of the developing and adult mouse cornea compared to the lens and tendon. *Exp Eye Res.* 87:214–225.
 33. Bonanno JA. 2012. Molecular mechanisms underlying the corneal endothelial pump. *Exp Eye Res.* 95:2–7.
 34. de Oliveira RC, et al. 2021. TGFbeta1 and TGFbeta2 proteins in corneas with and without stromal fibrosis: delayed regeneration of apical epithelial growth factor barrier and the epithelial basement membrane in corneas with stromal fibrosis. *Exp Eye Res.* 202:108325.
 35. Nishina S, et al. 1999. PAX6 expression in the developing human eye. *Br J Ophthalmol.* 83:723–727.
 36. Hatzfeld M, Keil R, Magin TM. 2017. Desmosomes and intermediate filaments: their consequences for tissue mechanics. *Cold Spring Harb Perspect Biol.* 9:a029157.
 37. Moll R, Divo M, Langbein L. 2008. The human keratins: biology and pathology. *Histochem Cell Biol.* 129:705–733.
 38. Kao WW. 2020. Keratin expression by corneal and limbal stem cells during development. *Exp Eye Res.* 200:108206.
 39. Yoshida S, et al. 2006. Cytokeratin 15 can be used to identify the limbal phenotype in normal and diseased ocular surfaces. *Invest Ophthalmol Vis Sci.* 47:4780–4786.
 40. Altshuler A, et al. 2021. Discrete limbal epithelial stem cell populations mediate corneal homeostasis and wound healing. *Cell stem cell.* 28:1248–1261.e1248.
 41. Govindarajan B, Gipson IK. 2010. Membrane-tethered mucins have multiple functions on the ocular surface. *Exp Eye Res.* 90:655–663.
 42. Martinez-Carrasco R, Argüeso P, Fini ME. 2021. Membrane-associated mucins of the human ocular surface in health and disease. *Ocular Surf.* 21:313–330.
 43. Zhou L, et al. 2020. ACE2 and TMPRSS2 are expressed on the human ocular surface, suggesting susceptibility to SARS-CoV-2 infection. *Ocular Surf.* 18:537–544.
 44. Collin J, et al. 2021. Co-expression of SARS-CoV-2 entry genes in the superficial adult human conjunctival, limbal and corneal epithelium suggests an additional route of entry via the ocular surface. *Ocular Surf.* 19:190–200.
 45. Shinde V, et al. 2021. Pathogenic alleles in microtubule, secretory granule and extracellular matrix-related genes in familial keratoconus. *Hum Mol Genet.* 30:658–671.
 46. Fischer S, Crow M, Harris BD, Gillis J. 2021. Scaling up reproducible research for single-cell transcriptomics using MetaNeighbor. *Nat Protoc.* 16:4031–4067.
 47. Cheng JB, et al. 2018. Transcriptional programming of normal and inflamed human epidermis at single-cell resolution. *Cell Rep.* 25:871–883.
 48. Birk DE. 2005. “Collagen Suprastructures” in collagen. In: *Topics in Current Chemistry.* Berlin, Heidelberg: Springer. p. 247.
 49. Abass A, Hayes S, White N, Sorensen T, Meek KM. 2015. Transverse depth-dependent changes in corneal collagen lamellar orientation and distribution. *J R Soc Interface.* 12:20140717.
 50. Tseng SC, Smuckler D, Stern R. 1982. Comparison of collagen types in adult and fetal bovine corneas. *J Biol Chem.* 257:2627–2633.
 51. Chakravarti S, et al. 1998. Lumican regulates collagen fibril assembly: skin fragility and corneal opacity in the absence of lumican. *J Cell Biol.* 141:1277–1286.
 52. Chaerkady R, et al. 2013. The keratoconus corneal proteome: loss of epithelial integrity and stromal degeneration. *J Proteomics.* 87:122–131.
 53. Wierzbicka-Patynowski I, Schwarzbauer JE. 2003. The ins and outs of fibronectin matrix assembly. *J Cell Sci.* 116:3269–3276.
 54. Murphy-Ullrich JE, Sage EH. 2014. Revisiting the matricellular concept. *Matrix Biol.* 37:1–14.
 55. Jester JV, et al. 1999. The cellular basis of corneal transparency: evidence for ‘corneal crystallins’. *J Cell Sci.* 112(Pt 5): 613–622.
 56. Zieske JD. 2004. Corneal development associated with eyelid opening. *Int J Dev Biol.* 48:903–911.
 57. Bourne WM. 2003. Biology of the corneal endothelium in health and disease. *Eye.* 17:912–918.
 58. Matthaei M, Meng H, Meeker AK, Eberhart CG, Jun AS. 2012. Endothelial Cdkn1a (p21) overexpression and accelerated senescence in a mouse model of Fuchs endothelial corneal dystrophy. *Invest Ophthalmol Vis Sci.* 53:6718–6727.
 59. Linsenmayer TF, et al. 1998. Development and roles of collagenous matrices in the embryonic avian cornea. *Prog Retin Eye Res.* 17:231–265.
 60. Shuttleworth CA. 1997. Type VIII collagen. *Int J Biochem Cell Biol.* 29:1145–1148.
 61. Joyce NC, Navon SE, Roy S, Zieske JD. 1996. Expression of cell cycle-associated proteins in human and rabbit corneal endothelium in situ. *Invest Ophthalmol Vis Sci.* 37:1566–1575.
 62. Bahn CF, et al. 1986. Postnatal development of corneal endothelium. *Invest Ophthalmol Vis Sci.* 27:44–51.
 63. Joyce NC, Harris DL, Mello DM. 2002. Mechanisms of mitotic inhibition in corneal endothelium: contact inhibition and TGF-beta2. *Invest Ophthalmol Vis Sci.* 43:2152–2159.
 64. Wilson SE, Sampaio LP, Shiju TM, Carlos de Oliveira R. 2021. Fibroblastic and bone marrow-derived cellularity in the corneal stroma. *Exp Eye Res.* 202:108303.
 65. Heissler SM, Sellers JR. 2014. Myosin light chains: teaching old dogs new tricks. *Bioarchitecture.* 4:169–188.
 66. Davis J, Duncan MK, Robison WG, Jr., Piatigorsky J. 2003. Requirement for Pax6 in corneal morphogenesis: a role in adhesion. *J Cell Sci.* 116:2157–2167.
 67. Song J, et al. 2003. Neonatal corneal stromal development in the normal and lumican-deficient mouse. *Invest Ophthalmol Vis Sci.* 44:548–557.
 68. Cvekl A, Tamm ER. 2004. Anterior eye development and ocular mesenchyme: new insights from mouse models and human diseases. *Bioessays.* 26:374–386.

69. Liu CY, *et al.* 1993. Cornea-specific expression of K12 keratin during mouse development. *Curr Eye Res.* 12:963–974.
70. Kabosova A, *et al.* 2007. Compositional differences between infant and adult human corneal basement membranes. *Invest Ophthalmol Vis Sci.* 48:4989–4999.
71. Norris RA, *et al.* 2007. Periostin regulates collagen fibrillogenesis and the biomechanical properties of connective tissues. *J Cell Biochem.* 101:695–711.
72. Zheng GX, *et al.* 2017. Massively parallel digital transcriptional profiling of single cells. *Nat Commun.* 8:14049.
73. Hao Y, *et al.* 2021. Integrated analysis of multimodal single-cell data. *Cell.* 184:3573–3587.e3529.
74. Satija R, Farrell JA, Gennert D, Schier AF, Regev A. 2015. Spatial reconstruction of single-cell gene expression data. *Nat Biotechnol.* 33:495–502.